International Journal of Multiphase Flow 35 (2009) 8–19

Contents lists available at ScienceDirect

International Journal of Multiphase Flow

journal homepage: www.elsevier.com/locate/ijmulflow

Flow and breakup characteristics of elliptical liquid jets

T.V. Kasyap, D. Sivakumar *, B.N. Raghunandan

Department of Aerospace Engineering, Indian Institute of Science, Bangalore 560 012, India

ARTICLE INFO

Article history:
Received 7 December 2007
Received in revised form 7 August 2008
Accepted 21 September 2008
Available online 27 September 2008

Keywords:
Elliptical liquid jets
Breakup
Instability
Axis-switching

ABSTRACT

This paper presents the results of an experimental study on liquid jets discharging from elliptical orifices into still ambient air. The experiments were conducted with a set of elliptical orifices of approximately same area of cross section but varying orifice aspect ratio using water and water–glycerol mixture as experimental fluids. The flow behavior of liquid jets was analyzed using their photographs captured by an imaging system. The measurements obtained for the elliptical liquid jets were compared with the circular liquid jets discharging from a circular orifice of the same area of cross section. Elliptical geometry of the orifice results in a flow process by which the emanating liquid jet periodically switches its major and minor axes as it flows downstream of the orifice. In this paper, we attempt to characterize the axis-switching process through its wavelength and amplitude. For a given elliptical orifice, the axis-switching process is dominantly seen in a particular range of flow conditions. The effects of the orifice aspect ratio and liquid viscosity on the axis-switching process are revealed through this study. The experimental results on jet breakup show that axis-switching process has a destabilizing effect on elliptical liquid jets within a particular range of flow conditions and it results in shorter breakup lengths compared to the circular jet. The extent to which axis-switching destabilizes the jet is dictated by the viscosity of liquid. An increase in orifice aspect ratio destabilizes elliptical liquid jets with low viscosity like water; however, this behavior seems to get obscured in water–glycerol mixture elliptical jets due to high viscosity.

1. Introduction

Liquid jet breakup is a ubiquitous phenomenon in nature and is a classic problem in hydrodynamics. It is commonly observed in spray and droplet formation processes encountered with several practical applications. Academic interest in the problem of liquid jet breakup dated back to the 19th century. Seminal contributions on the flow behavior of liquid jets discharging from circular and noncircular orifices came from the works of Bidone (1829), Savart (1833), Magnus (1855), Plateau (1873), Boussinessq (1877), Rayleigh (1879, 1945) and Chandrasekhar (1961). Delightful accounts of the earlier works on liquid jet breakup can be obtained from the comprehensive review articles by Bogy (1979) and Lin and Reitz (1998). Lord Rayleigh (1945) carried out a linear stability analysis of an infinite cylindrical column of inviscid liquid and concluded that such a liquid jet is unstable to axisymmetric disturbances of wavelength exceeding the circumference of the unperturbed liquid jet. Weber (1931) included the effects of viscosity and ambient medium in the analysis of liquid jet breakup and found that the effect of viscosity is to change the wavelength of the most unstable disturbance. Haenlien (1932) conducted experiments on liquid jet breakup with different liquids and circular orifices and constructed jet breakup length versus jet velocity curve (breakup curve) from the experimental measurements. Jet breakup length is the length of the coherent portion of the jet measured from the orifice exit plane (Grant and Middleman, 1966; Lin and Reitz, 1998). Breakup length of the circular jet increases linearly with jet velocity in a range of low jet velocities, reaches a peak or critical point, and thereafter decreases with increasing jet velocity. As jet velocity increases, the ambient atmosphere starts influencing the liquid jet and asymmetric waves or transverse waves begin to grow on the jet surface. Weber's theoretical analysis by considering the effect of ambient medium revealed a peak in the breakup curve (Weber, 1931), however, model predictions of the jet velocity at the peak or critical point did not match with experimental results (Grant and Middleman, 1966). It was concluded by Phinney (1972, 1973) that, immediately after the peak, the ambient medium causes a sharp increase in the amplification rate of disturbances on the liquid jet which reverses the increasing trend of breakup length variation as observed with experiments (Grant and Middleman, 1966). Further increase in the jet velocity earmarks the presence of short wavelength disturbances on the jet surface over a range of jet velocities and the breakup curve shows a positive slope in this regime (Lefebvre, 1989; Blaisot and Adeline, 2000). Breakup

* Corresponding author. Tel.: +91 80 22933022; fax: +91 80 23600134.
E-mail addresses: dskumar@aero.iisc.ernet.in, deivandren@yahoo.com (D. Sivakumar).

0301-9322/$ - see front matter © 2008 Elsevier Ltd. All rights reserved.
doi:10.1016/j.ijmultiphaseflow.2008.09.002

length soon reaches a maximum with increasing jet velocity and the liquid jet operates in the fully developed spray regime or the atomization regime at very high jet velocities.

Despite all these advances, there exist some subtle areas in this jet breakup problem which have not received adequate attention in past. For instance, effects of orifice geometry on the behavior of liquid jets have never been consistently taken into consideration (Lin and Reitz, 1998). A liquid jet emanating from an elliptical orifice switches its major and minor axes by right angles in a periodic manner as it flows downstream (Bidone, 1829; Rayleigh, 1879; Taylor, 1960). Surface tension causes the elliptical jet cross section to oscillate about a circular figure of equilibrium like a stretched membrane and consequentially the elliptical liquid jet executes multiple axis-switching (Rayleigh, 1879). Schematic sketches of free surface boundaries of a liquid jet discharging from an elliptical orifice are given in Fig. 1. Fig. 1(a) and (b) shows the appearance of elliptical liquid jet in the major axis plane and the minor axis plane of the elliptical orifice, respectively. The sketches also illustrate axis-switching phenomenon observed with the elliptical liquid jet. Once the jet ejects out of an elliptical orifice, surface tension force tries to minimize the curved surface area of the jet by pulling the ends of major axis inwards and pushing the ends of minor axis outwards. Due to the lateral inertia of the jet, the movements of major and minor axes ends do not stop abruptly at the ideal circular cross section, i.e., the cross section with minimum surface area, but overshoot. This causes the outward moving minor axis ends to be pushed further outwards and the inward moving major axis ends to be pulled further inwards. This kind of geometrical transformation superimposed with the axial motion of jet gives rise to the axis-switching profile on the jet as illustrated in Fig. 1. The axis-switching wavelength, λ_{as}, is defined as the distance measured between two consecutive crests or troughs as shown in Fig. 1. Rayleigh (1890) developed a mathematical model to calculate the dynamic surface tension of liquids from the axis-switching wavelength of elliptical liquid jets. This model was further improved by Bohr (1909). Analytical and numerical studies have been reported on elliptical liquid jets with and without surface tension to understand the spatial evolution of the free surface (Green, 1977; Geer and Strikwerda, 1980, 1983). Bechtel et al. (1988a,b, 1989) studied viscoelastic liquid jets issuing from elliptical orifices and predicted the axis-switching behavior of the liquid jets theoretically for the special case of Newtonian jet with constant surface tension. Later their model was extended to devise a technique for the measurement of dynamic surface tension and elongational viscosity of liquids (Bechtel et al., 1995).

Except the above conclusions on the free surface evolution of elliptical liquid jets, the fluid dynamic behavior of such liquid jets is largely overlooked in the literature. For instance published works on the breakup phenomena of liquid jets issuing from elliptical orifices is very scarce in the literature despite the fact that these orifices have already been studied for potential practical applications (McHale et al., 1971; Snyder et al., 1989). Hoyt and Taylor (1978) reported from their experiments that they were not able to identify any regular breakup on elliptical water jets. In this paper, we present experimental results on the breakup of liquid jets issuing from elliptical orifices of different aspect ratios using water and water–glycerol mixture as working liquids. Additional experiments were conducted with a circular orifice of approximately same cross sectional area as that of the elliptical orifices for the sake of comparison purposes. This paper is organized as follows. The experimental apparatus and procedure used in the study are given in the next section which is followed by the presentation and discussion of the experimental results. In Section 3, we first describe the visual observations on elliptical jets at various flow conditions, followed by the characterization of the axis-switching process in detail. We then proceed to describe the breakup curves of elliptical and circular jets of both liquids and present evidences to establish the role of axis-switching in the breakup of elliptical liquid jets. Finally, the major results arrived from the experimental study are listed in Section 5.

2. Experimental details

A set of stainless steel orifices containing one circular orifice and five elliptical orifices of various aspect ratios were used for the study. The geometric details of the orifices are given in Table 1. Cross sectional areas of all of these orifices were approximately same. Elliptical orifices were manufactured by electro-discharge machining process. Note that, owing to the fabrication processes, there were differences in the cross sectional area between elliptical orifices and the circular orifice and the measured error in this regard was estimated to be less than 5%. Sufficient care was taken to minimize the errors in obtaining the contour for elliptical orifices. The maximum deviation between the actual orifice contour and the ideal elliptical contour (the contour obtained based on the major and minor axes dimensions of the elliptical orifice) was estimated to be less than 0.078 mm (3.1% of D_o of the circular orifice) for all elliptical orifices used in the present study. The surface roughness of internal walls of the orifices was characterized by cutting a sample orifice longitudinally and examining it with

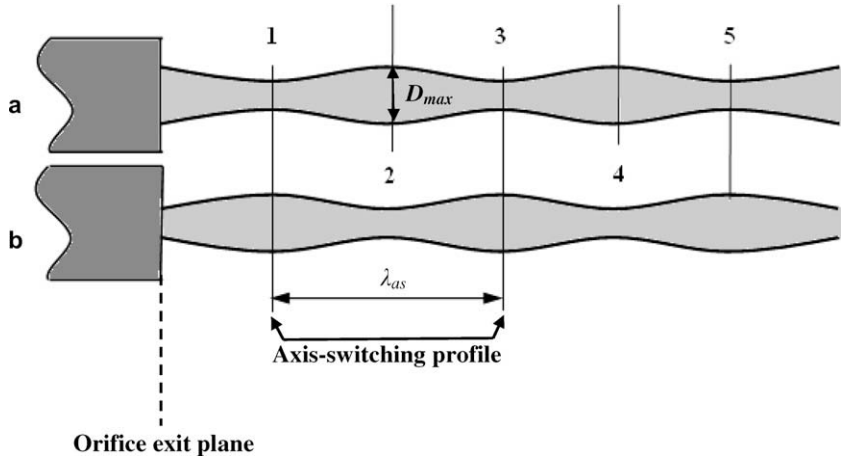

Fig. 1. Schematic sketches of an elliptical liquid jet discharging from an elliptical orifice. (a) Jet appearance in the major axis plane of the elliptical orifice, and (b) jet appearance in the minor axis plane of the elliptical orifice.

Table 1
Geometrical details for the orifices used in the present study

Elliptical orifices						Circular orifice			
Orifice index	Major axis (mm)	Minor axis (mm)	D_{eq}[b] (mm)	Length (mm)	Aspect ratio[a]	Orifice index	D_o (mm)	Length (mm)	Aspect ratio[a]
E1	3.02	2.04	2.48	25	1.48	C	2.51	25	1
E2	3.47	1.79	2.49	25	1.94				
E3	4.43	1.49	2.57	25	2.97				
E4	5.05	1.31	2.57	25	3.85				
E5	6.07	1.04	2.51	25	5.84				

[a] The ratio of major axis to minor axis of the orifice.
[b] The geometric mean of the major and minor axes of the elliptical orifice.

a stylus profilometer at various locations. The mean surface roughness of the internal walls of the orifices was found to be ranging from 0.8 to 1.48 μm. Fig. 2 illustrates the circular orifice and a sample of elliptical orifices used in the present study. During experimental runs, orifices were fixed in an assembly consisted of a cylindrical chamber of diameter 16 mm and length 50 mm and a converging section of circular cross section. Care was taken to avoid any sharp corner between the converging portion and the orifice passage entrance by rounding off the edge between them. The details of the entire orifice assembly are given in Fig. 3. A high-pressure liquid flow line comprised of a filter, a pressure gauge, and a control valve was used to supply experimental fluids from a large stainless steel tank to the orifice assembly. The volume of the tank (approximately 80 L) was large enough to neglect the orifice inlet pressure variations during experimental runs. Moreover, the tank was pressurized by means of a constant pressure, regulated, compressed air supply which ensured a constant orifice inlet pressure.

Experiments were carried out with two different liquids, water and a 1:1 mixture by volume of water and glycerol. The relevant physical properties of water–glycerol mixture have been taken from the literature (Yang and Leong, 2002) and are given in Table 2. Liquid flow rate from the orifice was estimated by measuring the volume of liquid collected in a measuring jar for a fixed time interval. The maximum error in the measurement of flow rate was estimated to be less than 3%. A Nikon D1X camera with a diffused backlighting system was used to take photographs of the jet. The imaging time was less than 15 μs. The pixel resolution of the camera was 2000 × 1312 with the viewing field ranging from 30 to 60 mm. A detailed description of the experimental setup used in this study can be obtained from Kasyap et al. (2008). Identical experimental procedure was followed for both circular and elliptical orifices except that for each elliptical orifice flow condition two sets of images were taken albeit at different instants, one with the camera viewing plane aligned with the major axis plane of the elliptical orifice and other with the minor axis plane of the elliptical orifice to correctly observe the axis-switching phenomenon.

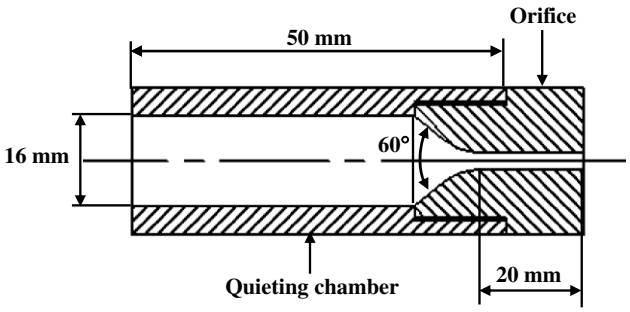

Fig. 3. A schematic of the orifice assembly.

The two normal views were not taken simultaneously because of the limitation of the experimental setup. Since axis-switching is a stationary phenomenon, the experimental procedure adopted in the present work did not restrict the analysis of axis-switching in any form. Due to the limitation of the field of view of the camera, for each flow condition several images of jets were captured at various axial locations from the orifice exit at different instants which were later patched together to obtain the complete picture of the intact jet without any spatial discontinuity. Captured images were analyzed by means of commercially available image processing software. In the present study, the jet breakup length is defined as the distance measured from the orifice exit to the point of the first break in the jet along the jet axis. Mean breakup length, L_b was estimated from the individual measurements of jet breakup length obtained from photographs available for each flow condition. The amplitude of axis-switching, D_{max}, defined as the width of jets measured in the major axis plane, was also obtained from the photographs. In a similar manner the measurement of axis-switching wavelength, λ_{as} was also obtained from the photographs. Sufficient care was taken to ensure the repeatability of experimental measurements. For each flow condition, experiment was repeated from 8 to 15 times and mean and standard deviation of

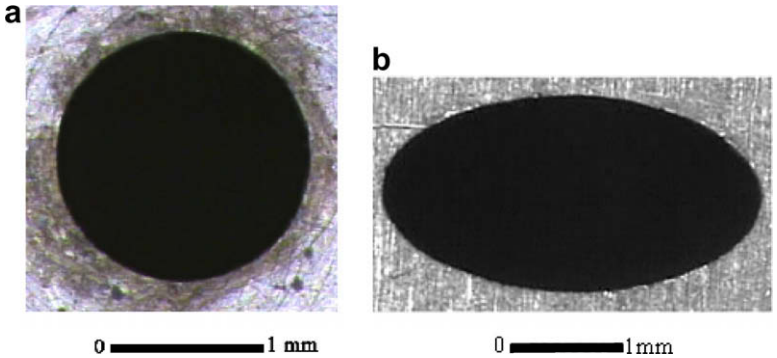

Fig. 2. Typical high resolution images of orifices used in the present study. (a) Circular orifice C, and (b) elliptical orifice E2.

Table 2
Properties of working fluids

Working fluid	ρ_l (kg/m^3)	μ_l (kg/m/s)	σ (N/m)
Water	995	0.802×10^{-3}	0.0728
Water–glycerol mixture (1:1 by volume)	1107	6.01×10^{-3}	0.0669

Table 3
Maximum standard deviation of measured parameters

Liquid	Measured quantities	*We*	Range of measured values (cm)	Maximum standard deviation (cm)
Water	λ_{as}	<30	<1.5	0.07
		30–225	1.5–3.0	0.10
	D_{max}	4–100	0.2–0.4	0.02
Water–glycerol mixture	λ_{as}	<15	<1.2	0.1
		15–400	1.2–5.0	0.4
	D_{max}	10–625	0.2–0.4	0.01

various measured quantities were calculated subsequently. The standard deviation for the measurements of axis-switching wavelength and the amplitude of axis-switching at different *We* ranges for both liquids are given in Table 3.

Flow conditions of liquid jets were expressed in terms of nondimensional numbers such as Weber number, *We*, Reynolds number, *Re* and Ohnesorge number, *Oh* which were estimated from

$$We = \frac{\rho_l U_o^2 D}{\sigma}, \tag{1}$$

$$Re = \frac{\rho_l U_o D}{\mu_l}, \tag{2}$$

$$Oh = \frac{\mu_l}{\sqrt{\rho_l D \sigma}}, \tag{3}$$

where ρ_l is the liquid density, U_o, the mean axial velocity of the liquid jet at the orifice exit; D, the flow geometrical scale; μ_l, the liquid viscosity, and σ, the surface tension. The value of D for the circular and the elliptical orifices was taken as D_o, the orifice exit diameter, and D_{eq}, the geometric mean diameter of the elliptical orifice, respectively. The values of U_o were estimated from the volume flow rate and the orifice exit area. In the present study, the ranges of values of *We* and *Re* for water jets were 0.8–13,300 and 450–61,000, respectively. The corresponding values for water–glycerol mixture jets were 0.28–1300 and 36–2300. *Oh* numbers for water jet and water–glycerol mixture jets were 0.0019 and 0.0139, respectively.

3. Results

3.1. Visual observations of elliptical liquid jets with different flow conditions

Experimental data obtained for liquid jets discharging from elliptical orifices reveals that elliptical liquid jets show distinct flow features in different ranges of flow conditions. Fig. 4(a)–(c) shows images of water jets discharging from the elliptical orifice E3 for different low $\sqrt{We}$ in the range of 0.86–1.49. For each *We*, a pair of images are given in which the top one corresponds to the major axis plane and the bottom one to the minor axis plane of the elliptical orifice. The jet width appears to be same in both images for all *We* except in the vicinity of the orifice exit. A comparison of the major axis and minor axis images for each *We* given in Fig. 4 reveals that the elliptical jet does not exhibit the axis-switching phenomenon. Instead it degenerates to a circular jet immediately after exiting from the orifice. The dominance of surface tension forces at these low *We* conditions compels the jet to take a circular cross section to minimize its surface energy and leads to the suppression of axis-switching process. At locations far away from the orifice exit, an elliptical jet develops symmetric radial deformations on its surface and breaks into drops in the exact manner of the Rayleigh breakup of a circular liquid jet (Rayleigh, 1945). Fig. 4(d) shows the image of a water jet discharging from the circular orifice C for $\sqrt{We} = 1.42$ which falls within the range of *We* conditions given in Fig. 4(a)–(c). It is interesting to observe from the images given in Fig. 4 that the flow behavior of elliptical liquid jets at these *We* conditions resembles that of a circular liquid jet and lacks the influence of orifice shape.

As *We* increases, the lateral inertia of the elliptical liquid jet also increases and becomes comparable to its surface tension force. At this point, according to Rayleigh (1879), the free surface of the jet behaves like a stretched membrane which executes oscillations in the lateral direction about a circular figure of equilibrium and develops axis-switching. Fig. 5 illustrates the flow behavior of elliptical water jets at moderate $\sqrt{We}$ values falling in the range of 3.93–10.58. A comparison of the free surface of elliptical jets seen in the near region of the orifice exit between the major axis and minor axis images for each *We* reveals that the elliptical jet switches its axes as it flows downstream. The switching process is found to be periodic particularly in the lower band of *We* values given in Fig. 5. At still higher *We*, the free surface of elliptical jet is not as smooth as seen at lower *We* probably due to other influencing parameters, like turbulence or the ambient medium. Fig. 6

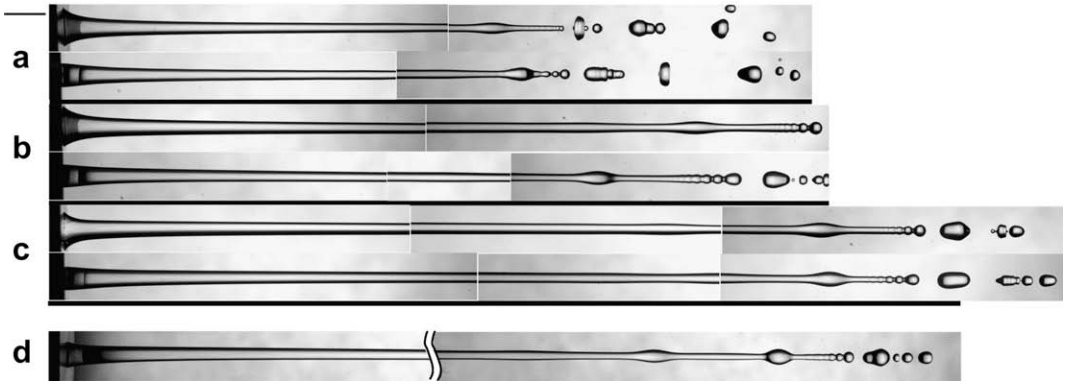

Fig. 4. Images (a)–(c) of water jets discharging from the elliptical orifice E3 at three different $\sqrt{We}$ conditions: (a) 0.86, (b) 1.12, and (c) 1.49. For each flow condition a pair of images is given: the top one corresponds to the case in which the camera viewing plane was aligned with the major axis plane of the elliptical orifice and the bottom one to the minor axis plane of the elliptical orifice. (d) Image of water jet discharging from the circular orifice C at $\sqrt{We} = 1.42$. The line segment shown on the left top corner of the figure indicates a scale distance of 5 mm.

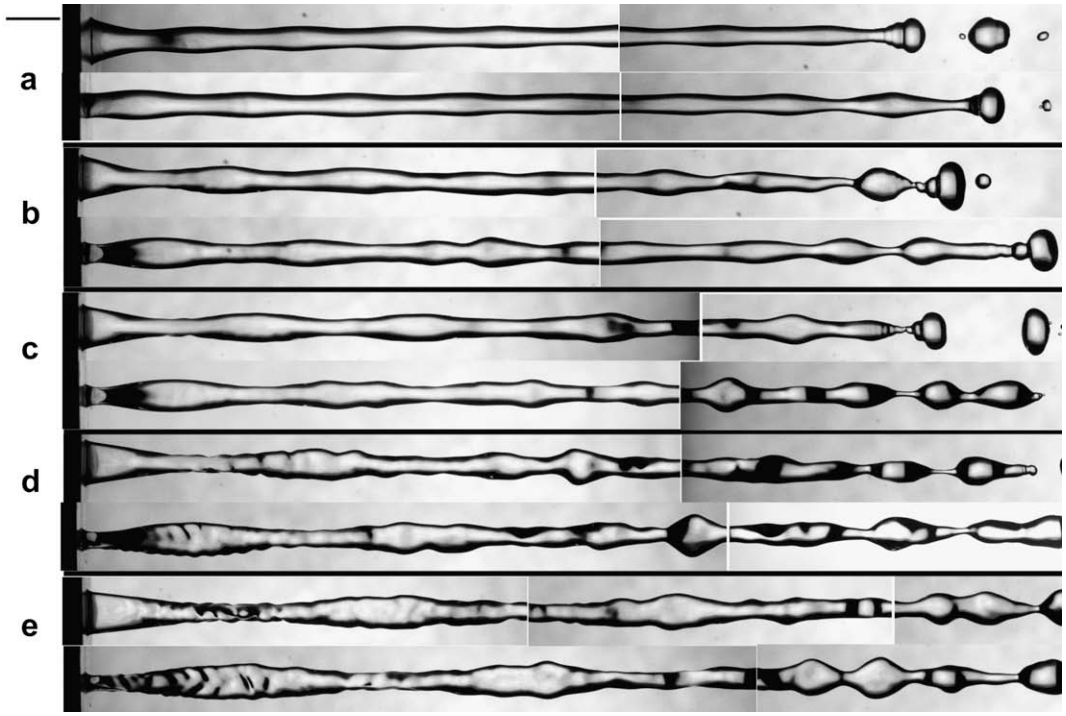

Fig. 5. Images of water jets discharging from the elliptical orifice E3 at different moderate values of $\sqrt{We}$: (a) 3.93, (b) 5.45, (c) 6.35, (d) 8.06, and (e) 10.58. All other details remain same as in the caption of Fig. 4.

illustrates water jets discharging from the elliptical orifice E3 for different high $\sqrt{We}$ values falling in the range of 18–31. The ruffling of the jet surface at these *We* conditions is evident from the images given in Fig. 6 which hinders the precise identification of axis-switching segments.

The experimental observations on the flow behavior of elliptical water jets hold good for the elliptical water–glycerol mixture jets studied here except the significant viscous damping of the axis-switching process and the suppression of ruffling on the jet surface at higher *We* present in the latter. Fig. 7 shows the viscous damping of axis-switching of the water–glycerol mixture jet issuing from the elliptical orifice E4 at $We = 39.26$. The amplitude of axis-switching decreases drastically along the jet and at larger distances from the orifice exit the elliptical jet degenerates to a circular liquid jet. Owing to the higher viscosity, no ruffling is seen on the free surface of water–glycerol jets at higher *We*. This is clear from Fig. 8 which illustrates images of water and water–glycerol mixture jets discharging from the elliptical orifice E3 for $We \approx 330$.

3.2. Characterization of the axis-switching phenomenon

The axis-switching phenomenon of elliptical liquid jets is characterized in the present study by the wavelength of axis-switching (λ_{as}) and its amplitude or length of major axis (D_{max}). The measurements of λ_{as} and D_{max} for water jets were limited to a relatively narrow range of *We* compared to water–glycerol mixture jets due to the formation of ruffles on water jets and difficulty in determining the axis-switching segments precisely. The variation of λ_{as}/D_{eq} with $\sqrt{We}$ for both water jets and water–glycerol mixture jets discharging from elliptical orifices of various aspect ratios is given in Fig. 9. The value of λ_{as} for a given *We* presented in this plot corresponds to the mean value of all measurable wavelengths seen in the entire jet. For both water and water–glycerol mixture jets, there exists a lower limit of $\sqrt{We}$ below which axis-switching was impossible to be perceived. In the case of water jets, measurements of λ_{as} were limited by a $\sqrt{We}$ above which precise measurement was impossible due to the presence of ruffles on the jet surface. The plots of λ_{as}/D_{eq} for both water and water–glycerol mixture jets show a linear variation which is consistent with the previous observations (Rayleigh, 1879; Geer and Strikwerda, 1983). The linear trend of λ_{as}/D_{eq} with $\sqrt{We}$ holds true for all orifice aspect ratios and the orifice aspect ratio does not seem to influence λ_{as}/D_{eq} for moderate values of the orifice aspect ratio because all curves collapse to a reasonable extent. However, an examination of the slope of the curves given for water jets in Fig. 9 reveals a deviation in slope for the data obtained for the elliptical orifices with high orifice aspect ratio, especially at higher *We*. Elliptical jets discharging from orifices with high aspect ratios exhibit distortion in their elliptical cross section (Bechtel et al., 1995) which may alter the axis-switching wave length. The effect of viscosity on λ_{as} can be understood from Fig. 9. Since all data points of water jets and water–glycerol mixture jets collapse into a single in Fig. 9 line

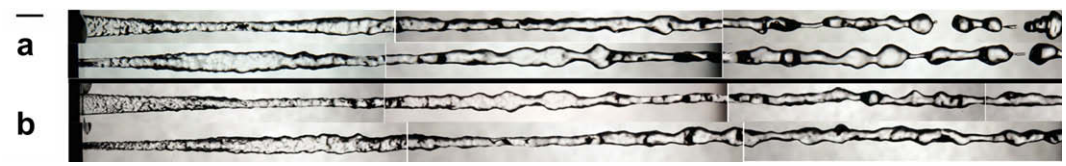

Fig. 6. Images of water jets discharging form the elliptical orifice E3 at different high $\sqrt{We}$ conditions: (a) 18.35 and (b) 30.34. All other details remain same as in the caption of Fig. 4.

Fig. 7. Image of water–glycerol mixture jet discharging from the elliptical orifice E4 at $We = 39.26$. All other details remain same as in the caption of Fig. 4.

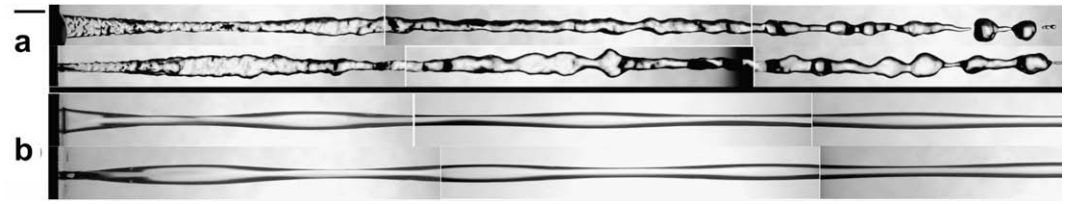

Fig. 8. Images of water jet and water–glycerol mixture jet discharging from the elliptical orifice E3 for $We \approx 330$. (a) Water jet and (b) water–glycerol mixture jet. The Ohnesorge numbers are 0.0019 and 0.0139, respectively, for (a) and (b). All other details remain same as in the caption of Fig. 4.

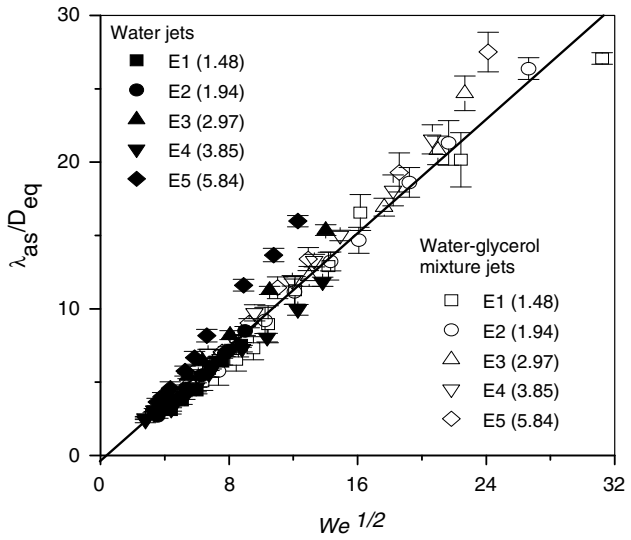

Fig. 9. Variation of nondimensionalized axis-switching wavelength, λ_{as}/D_{eq} with $\sqrt{We}$ for water jets and water–glycerol mixture jets discharging from the elliptical orifices with different orifice aspect ratio. The solid line is the linear fit of the entire data. The error bar for each data point indicates one standard deviation towards both directions from the mean.

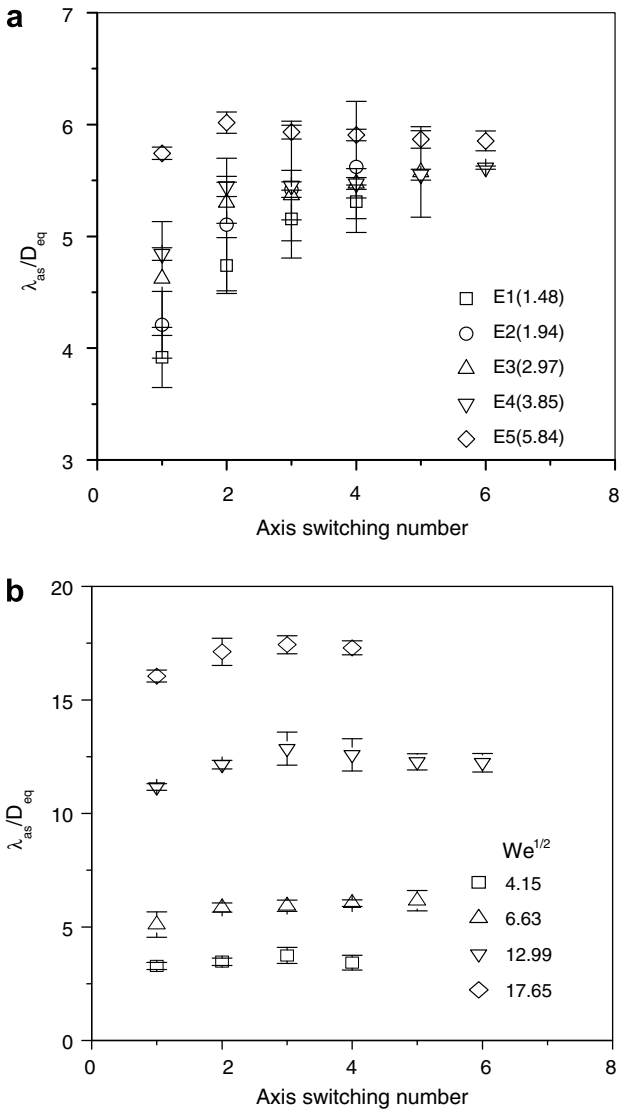

Fig. 10. Variation of nondimensionalized axis-switching wavelength, λ_{as}/D_{eq} with axis-switching number for water–glycerol mixture jets. (a) For jets issuing from various elliptical orifices at a $\sqrt{We} = 6.0$, and (b) for jets issuing from E3 with various $\sqrt{We}$.

we can conclude that the wavelength of axis-switching is independent of the viscosity also.

The variation of λ_{as} along the axis of the jet is important since some of the previous studies have reported its consequences while measuring the dynamic surface tension (Bohr, 1909). The measurement of λ_{as} along the axis of the jet has been attempted only for water–glycerol mixture jets since the ruffles developing on water jets at larger axial distances from the orifice exit makes the accurate measurement of λ_{as} impossible. Measured values of λ_{as} along the axis of water–glycerol mixture jets have been plotted in Fig. 10 in the nondimensional form. The abscissa of the plot is the axis-switching number as shown in Fig. 1. Fig. 10(a) illustrates the axial variation of λ_{as} for the elliptical orifices of various aspect ratios around a $\sqrt{We}$ of 6.0 and Fig. 10(b) depicts the axial variation of λ_{as} for the elliptical orifice E3 at various $\sqrt{We}$ conditions. Axis-switching wavelength is initially low and it increases to almost a constant value. This is in agreement with the previously observed trends by Bohr (1909). Two effects may contribute to the axial-variation of λ_{as}: one is the gravitational acceleration, g of the jet and other is the presence of the orifice. To reveal the effect of gravity, Froude number, Fr defined by

$$Fr = \frac{U_0^2}{gD_{eq}} \tag{4}$$

has been calculated for flow conditions shown in the plots. Estimated value of *Fr* ranges from 10 to 850, indicating that the flow is dominated by inertia. Moreover, if gravitational acceleration affects λ_{as}, a continuous increase in λ_{as} is to be expected since the jet velocity continues to increase along the jet axis. However, the plots given in Fig. 10 do not show such a continuous variation. Therefore, the plausible cause for the variation of λ_{as} near the orifice may be the presence of orifice itself. Small irregularities involved in the formation of the jet, like an imperfection in the contour of the orifice, may cause a change in λ_{as} near the orifice, which later dies out at larger distances from the orifice, yielding a nearly constant λ_{as}. This point was considered by Bohr (1909). However, a rigorous study is required to ascertain these facts.

The variation of D_{max}/D_{eq} given in Fig. 11(a) and (b) for water and water–glycerol mixture jets, respectively, shows a monotonic increase with $\sqrt{We}$. The value of D_{max} given in these figures corresponds to the jet width measured at the first crest of the major axis image of the jet as illustrated in Fig. 1. The monotonic variation of D_{max}/D_{eq} with $\sqrt{We}$ is understandable since an increase in *We* apparently increases the lateral inertia of the jet which results in the increase in the magnitude of overshooting of the jet major axis. In contrast to the variation of λ_{as}/D_{eq} given in Fig. 9, the orifice aspect ratio shows a remarkable effect on the nondimensionalized amplitude. For a given flow condition, an increase in orifice aspect ratio causes an increase in amplitude also. Superimposed curves of D_{max}/D_{eq} versus $\sqrt{We}$ for water and water–glycerol mixture jets issuing from a typical elliptical orifice are shown in Fig. 11(c). It is obvious from the plot that for the same flow condition, the amplitude of axis-switching of water–glycerol liquid jet is less than that of the water jet. This is due to intense viscous damping present in water–glycerol mixture jets. The same trend has been found for other aspect ratios also.

Further insights about the effect of viscous damping on D_{max} can be obtained by nondimensionalizing the measurements of D_{max} given in Fig. 11(a) and (b) with the major axis dimension of the elliptical orifice, $D_{o,major}$ to yield the quantity $D_{max}/D_{o,major}$. Physically this quantity represents the extent to which D_{max} recovers to the major axis dimension of the particular elliptical orifice. If gravity is neglected and jet is of an inviscid liquid, then D_{max} should always recover to the major axis dimension of the orifice $D_{o,major}$, thus making the value of $D_{max}/D_{o,major}$ equal to unity. However, in real cases, due to the viscous damping of axis-switching and the presence of gravitational acceleration, $D_{max}/D_{o,major}$ will always be less than unity. To study the effect of the orifice aspect ratio on $D_{max}/D_{o,major}$, the variation of $D_{max}/D_{o,major}$ with $\sqrt{We}$ is plotted for each orifice aspect ratio in Fig. 12(a) and (b). The former is for water jets and the latter is for water–glycerol mixture jets. It is obvious from Fig. 12(a) and (b) that liquid jets issuing from orifices of larger aspect ratios show smaller values of $D_{max}/D_{o,major}$ and therefore recover less than those issuing from orifices of lower aspect ratios. The nature of the amplitude decay along the jet axis is more or less exponential. Fig. 13 illustrates the exponential nature of amplitude decay of water–glycerol mixture jet emanating from the elliptical orifice E4. The solid curve in Fig. 13 fits the variation of amplitude with axis-switching number without considering the amplitude of the zeroth axis-switching which is the major axis dimension of the elliptical orifice, $D_{o,major}$. If $D_{o,major}$ is introduced in the data set, the same exponential curve does not fit the experimental measurements. In other words, between the orifice exit and the first crest of the axis-switching profile in the major axis plane, the amplitude decay is no longer same as the exponential decay observed afterwards. A similar trend has been observed with other aspect ratios also. This shows the possible role of the orifice exit conditions on the amplitude of axis-switching, similar to the effect of orifice exit on the axis-switching wavelength.

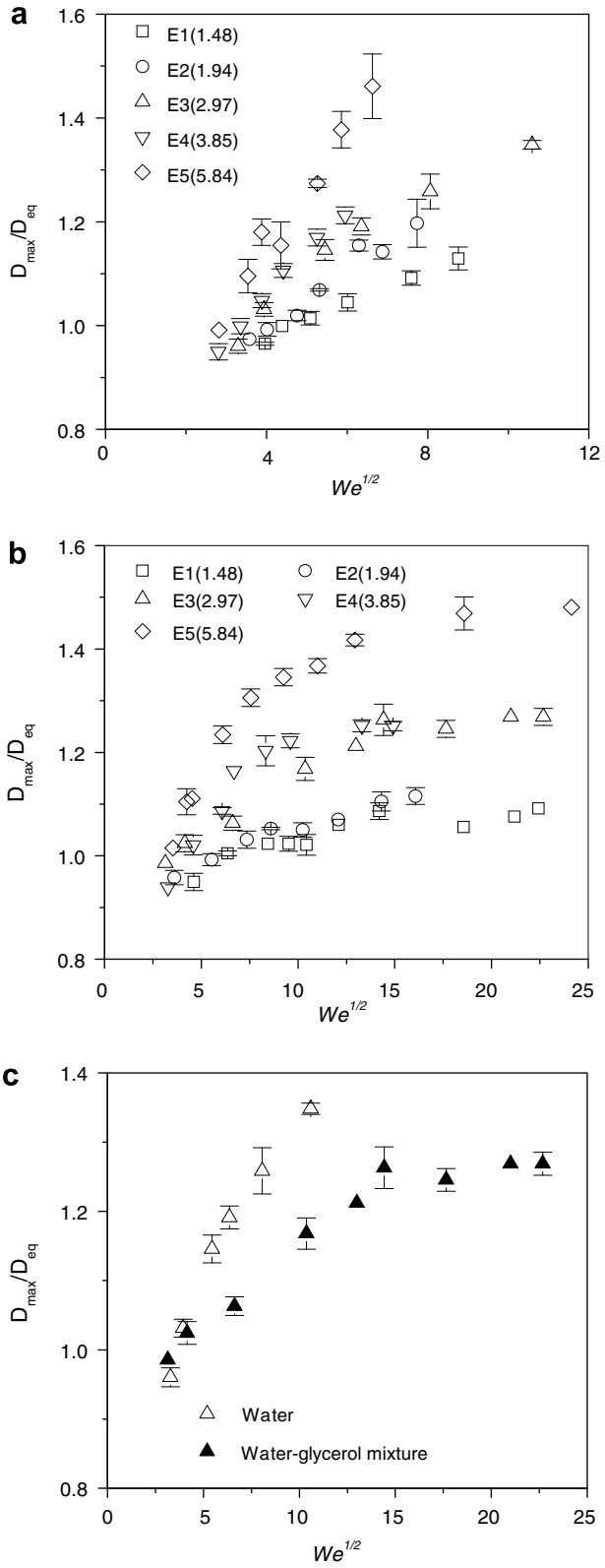

Fig. 11. Variation of nondimensionalized axis-switching amplitude, D_{max}/D_{eq} with $\sqrt{We}$. (a) Elliptical water jets, (b) elliptical water–glycerol mixture jets, and (c) water and water–glycerol mixture jets issuing from the elliptical orifice E3 together.

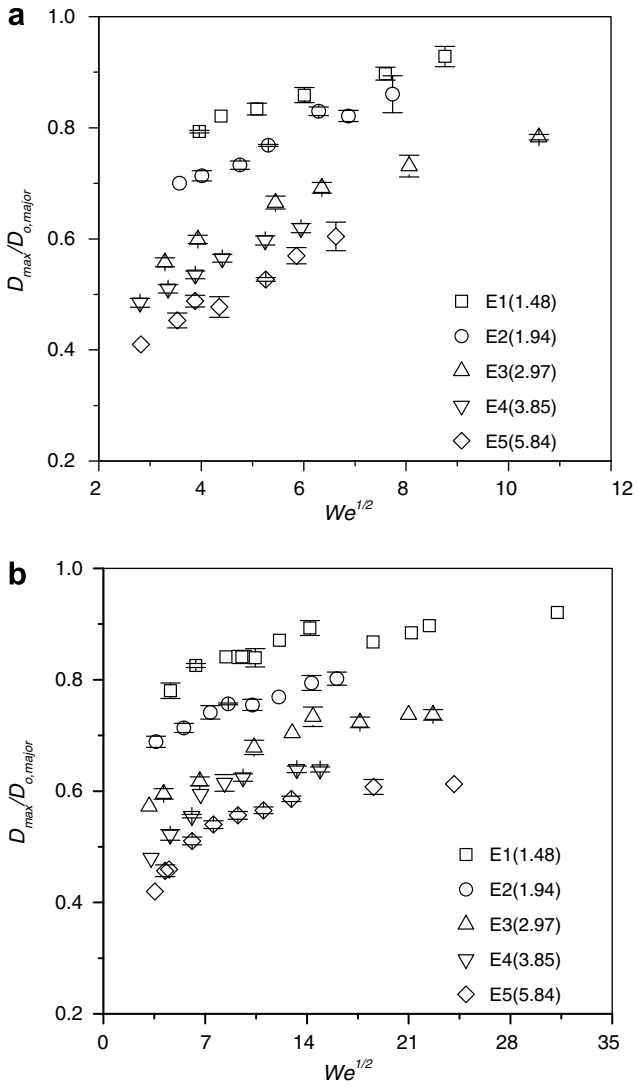

Fig. 12. Variation of $D_{max}/D_{o,major}$ with $\sqrt{We}$. (a) Elliptical water jets, and (b) elliptical water–glycerol mixture jets issuing from various orifices.

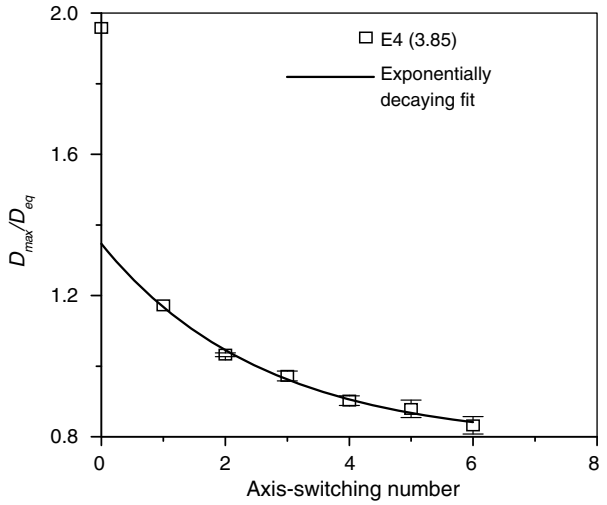

Fig. 13. Variation of D_{max}/D_{eq} with axis-switching number for water–glycerol mixture jets discharging from the elliptical orifice E4. The solid curve shows the exponential decay of D_{max}/D_{eq} with axis-switching number.

3.3. Breakup of elliptical liquid jets

Measurements of the mean breakup length, L_b of the jet were obtained for the water jets discharging from the circular and elliptical orifices with different flow conditions. Fig. 14 shows the variation of L_b/D_{eq} for water jets discharging from the circular and elliptical orifices for the whole range of *We* and Fig. 15 depicts the same for water–glycerol mixture jets. For a clear view of the nature of breakup curves in the lower range of *We* of water jets, a portion of the breakup curves falling in the $\sqrt{We}$ range of 0–20 has been magnified and inserted in Fig. 14. The data identified by filled symbols in Figs. 14 and 15 corresponds to the variation of L_b/D_{eq} for the circular liquid jets, which shows a linear variation at first, reaches a peak and thereafter decreases with increasing *We*. This trend in the breakup curve for liquid jets discharging from the circular orifice C is in agreement with the previous works (Grant and Middleman, 1966; Lefebvre, 1989; Blaisot and Adeline, 2000; Sterling and Sleicher, 1975) discussed in Section 1. The data identified by open symbols in Figs. 14 and 15 corresponds to the variation of L_b/D_{eq} for jets discharging from the elliptical orifices with different aspect ratio. At very low *We*, the breakup curves of elliptical jets for all orifice aspect ratios tend to merge along line A–A as shown in the inset of Figs. 14 and 15. It indicates that the orifice geometry (elliptical orifice shape) does not influence the breakup of elliptical liquid jets at very low *We*. Images given in Fig. 4(a)–(c) correspond to flow conditions falling on the line A–A. Absence of axis-switching causes elliptical jets to behave in a similar manner to that of the equivalent circular jet, which explains the collapse of breakup curves at low *We*. The line B–B shown in the inset of Figs. 14 and 15 joins points where the axis-switching starts to become clearly visible for elliptical jets and it continues to be visible in the region lying to the right of the line B–B. For the region lying to the left of the line B–B, the axis-switching is not clearly visible. Thus the transition of elliptical jets from no axis-switching mode to axis-switching mode occurs between the line A–A and the line B–B. Fig. 16(a) and (b) portray the flow behavior of elliptical water jets and water–glycerol mixture jets, respectively, in the transition regime with different *We*. In the case of water jets given in Fig. 16(a) axis-switching starts to become visible in the forth image. The fifth image lies in a flow condition which is immediately beyond the transition regime. The respective images for water–glycerol mixture jets are the third and forth of Fig. 16(b). A close observation of the breakup curves given in the inset of Fig. 14 reveals that, as *We* increases, breakup curves for elliptical jets start deviating from the line A–A and they soon reach a peak and encounter a change in slope. The peaks, hereafter, will be called as critical points. As seen in the inset of Fig. 14, the critical point and the associated slope change in the breakup curves of elliptical jets occur between the lines A–A and B–B. Thus the transition regime of elliptical jets from no axis-switching mode to axis-switching mode is characterized by a change of slope in their breakup curves. The change of slope is more conspicuous in the case of water jets than in the case of water–glycerol mixture jets whose breakup curves are given in Fig. 15. However, Fig. 17 reveals that the change of slope is indeed present in the case of water–glycerol mixture jets. Within the transition regime, after the critical points, the breakup lengths of elliptical jets are significantly lesser than that of the equivalent circular jet. This trend continues after the line B–B till the line C–C in Figs. 14 and 15. Lower breakup lengths of elliptical jets indicate that elliptical jets are more unstable than the equivalent circular jet. Within this zone of enhanced instability, increasing aspect ratio for a given *We*, destabilizes water jets further as seen in Fig. 14. However, such a destabiliz-

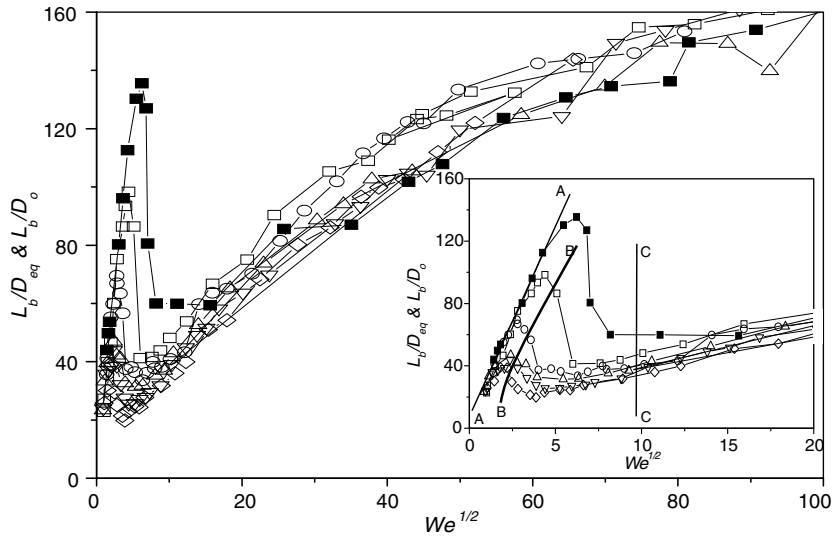

Fig. 14. Breakup curves (variation of the nondimensionalized breakup length, L_b/D_o and L_b/D_{eq} against $\sqrt{We}$) for water jets. The inset shows the magnified view of the breakup curves in the lower range of $\sqrt{We}$, 0–20. The symbols used in the plot denote the following: ■, C (1); □, E1 (1.48); ○, E2 (1.94); △, E3 (2.97); ▽, E4 (3.85); and ◇, E5 (5.84).

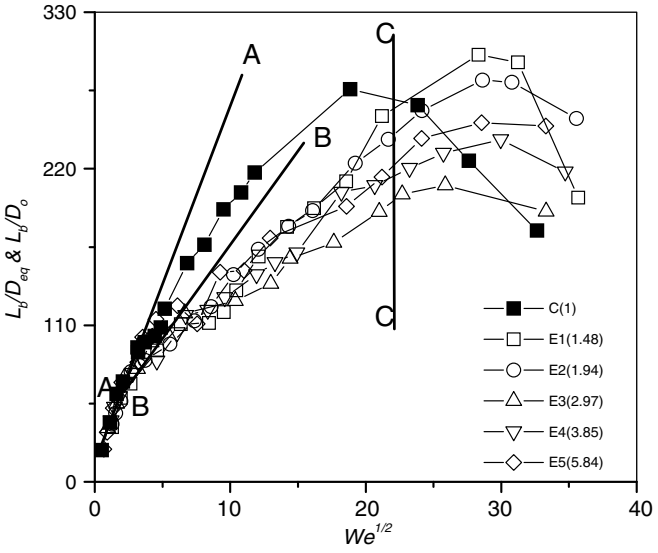

Fig. 15. Breakup curves (variation of the nondimensionalized breakup length, L_b/D_o and L_b/D_{eq} against $\sqrt{We}$) for water–glycerol mixture jets.

ing effect of orifice aspect ratio has not been observed with relatively more viscous water–glycerol mixture jets (refer Fig. 15).

For further analysis we consider the *We* at which the slope change takes place in the breakup curve, referred as the critical point, and the *We* where axis-switching starts to become visible. These are denoted by $\left(\sqrt{We}\right)_{crit}$ and $\left(\sqrt{We}\right)_{min}$, respectively. Both $\left(\sqrt{We}\right)_{crit}$ and $\left(\sqrt{We}\right)_{min}$ are found to be nearly matching in the case of water jets. Details of this method of analysis of the breakup curves can be found in Kasyap et al. (2008). A similar analysis on water–glycerol mixture jets revealed remarkable agreement between $\left(\sqrt{We}\right)_{crit}$ and $\left(\sqrt{We}\right)_{min}$. In both cases, most of the time, an exact numerical equality was not found. This is indeed so since the determination of the $\left(\sqrt{We}\right)_{min}$, where axis-switching starts to become visible, is more or less subjective. The above analysis suggests that the critical point and the associated change in the breakup curves of elliptical jets may be due to the onset of axis-switching. To confirm this hypothesis further we made attempts to understand the effect of ambient medium on the breakup of elliptical liquid jets at flow conditions near the critical point. Note that the critical point occurs even in the case of circular jets and most of the time it is caused by the ambient medium (Phinney, 1973). Earlier studies of circular jets show that the effect of ambient medium on the jet breakup is negligible if the gas Weber number, $We_g < 0.4$ (Pan and Suga, 2006; Reitz, 1978). The gas Weber number, We_g is defined by the relation

$$We_g = \frac{\rho_g U_o^2 D}{\sigma}, \tag{5}$$

where ρ_g is the density of the ambient gas. The values of We_g evaluated at the critical conditions for the elliptical jets studied here lie in the range of 0.0024–0.045 which is significantly lower than 0.4 and hence rules out the role of ambient medium at the critical point seen in the breakup curves of elliptical water jets as well as water–glycerol mixture jets. The critical point on the breakup curve earmarks the onset of the enhanced instability found in elliptical jets. Note that within this regime of enhanced instability, axis-switching is dominantly perceivable on both water and water–glycerol mixture jets. These findings reveal that the effect of axis-switching on elliptical jets is to destabilize them further since it reduces their breakup length significantly compared to that of the equivalent circular jet under the same flow conditions.

The influence of elliptical orifice geometry on the breakup of liquid jet ceases to exist beyond the line C–C in Figs. 14 and 15 though axis-switching is seen at these flow conditions on both elliptical water jets and water–glycerol mixture jets. The increasing trend of the breakup length of the circular water jet with *We* in Fig. 14, shown by filled symbols, agrees with the previous observations (Grant and Middleman, 1966). Photographs of elliptical water jets at these flow conditions (Fig. 6) show considerable ruffling on the jet surface which suggests that the flow is no longer laminar. Estimated values of *Re* of water jets at these flow conditions range from 7500 to 61,000 which shows that turbulence is weakly developed. The values of We_g estimated at these flow conditions lie in the range 0.26–12 which indicates a strong influence of ambient medium on the jet breakup (Pan and Suga, 2006; Reitz, 1978). The effect of axis-switching on

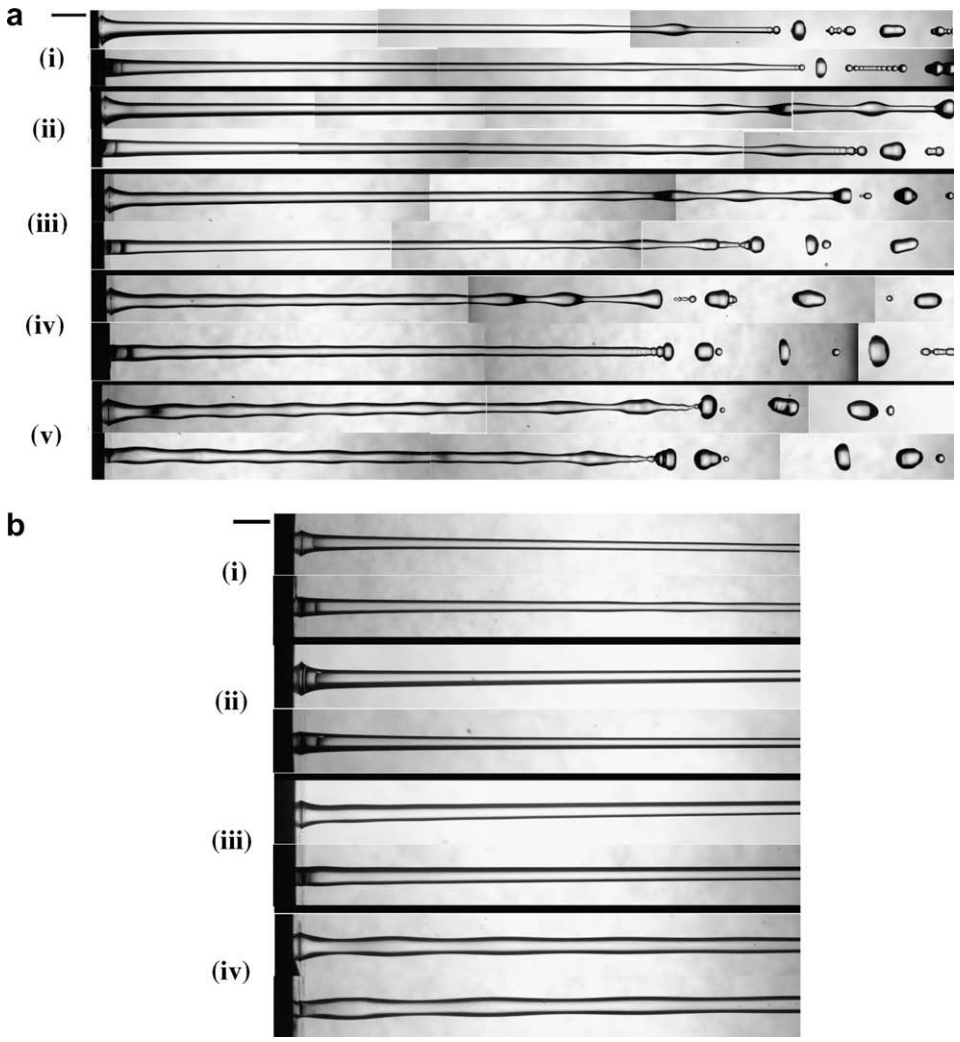

Fig. 16. Images of elliptical water and water–glycerol mixture jets in the transition regime. (a) Water jet issuing from E3 with $\sqrt{We}$: (i) 1.49, (ii) 2.40, (iii) 2.77, (iv) 3.28, and (v) 3.94. Image (v) was taken at a flow condition lying immediately after the transition regime. (b) Water–glycerol mixture jets issuing from the elliptical orifice E2 with $\sqrt{We}$: (i) 1.91, (ii) 2.67, (iii) 3.71, and (iv) 5.53. The flow condition for image (iv) lies immediately after the transition regime. All other details remain same as in the caption of Fig. 4.

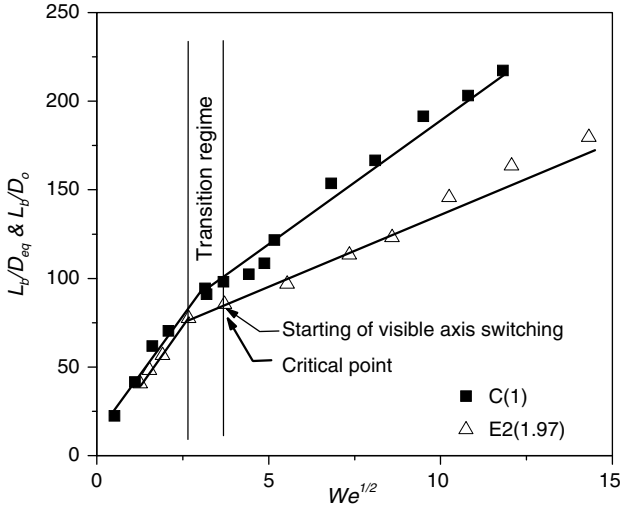

Fig. 17. Breakup curve for the water–glycerol mixture jet issuing from the elliptical orifice E2 and circular orifice C to illustrate the change of slope at the critical point.

the jet breakup may get undermined by the influence of ambient medium and jet turbulence which can cause the breakup curves to merge together after the line C–C. All elliptical water–glycerol mixture jets exhibit a peak after the line C–C as seen in Fig. 15 and asymmetric breaking was observed in these flow conditions. Note that at larger distances from the orifice exit, elliptical water–glycerol mixture jets behave effectively like circular jets due to the damping of the axis-switching process. Ambient medium causes these degenerated elliptical jets to breakup in an asymmetric manner, like in the case of circular jets at high *We* conditions. Gas Weber number We_g evaluated in this regime ranges from 0.65 to 1.66 which clearly indicates the influence of ambient atmosphere near the peak.

An interesting observation on water jets issuing from elliptical orifices of larger aspect ratios is that at larger *We*, transverse waves develop in the vicinity of the first switching observed from the major axis viewing plane of the elliptical orifice. This is illustrated in Fig. 18, which shows the images of water jets discharging from the elliptical orifice E5 with orifice aspect ratio 5.84, at various *We* conditions. The regions surrounded by rectangles marked in the images given in Fig. 18 indicate the presence of transverse waves on the jet surfaces. Note that, at the same axial location in the minor axis images, no transverse waves are seen. A comparison of the jet width at these locations between the major and minor axis images indicates that, the jet width is significantly larger in

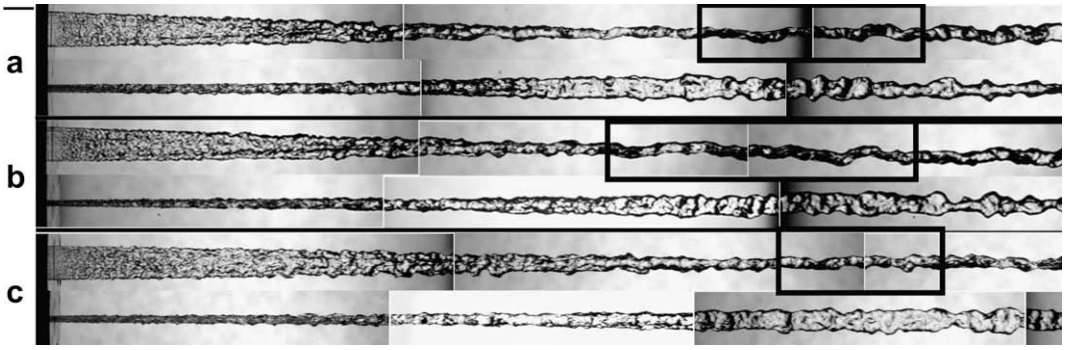

Fig. 18. Images of water jets discharging from the elliptical orifice E5 at various *We* conditions. The values of *We* are: (a) 3310, (b) 4300, and (c) 6450. Transverse waves are observed only in the major axis plane images and their locations are marked by rectangles. All other details remain same as in the caption of Fig. 4.

the minor axis plane than in the major axis plane. Thus the elliptical jet effectively behaves like a thin sheet whose plane is perpendicular to the major axis plane of the elliptical orifice. This liquid sheet then tends to develop transverse waves similar to waves seen on plane liquid sheets.

4. Discussion: role of axis-switching

The experimental results of water and water–glycerol mixture jets given in the previous sections clearly show that the onset of axis-switching process results in a significant reduction of the breakup length of elliptical liquid jets compared to that of the equivalent circular liquid jets. This destabilizing effect of axis-switching on liquid jets can be understood further via the following arguments. It is known that the free surface of a liquid jet always seek configurations with minimum surface energy for a given volume. This makes a cylindrical liquid jet or a liquid ligament spontaneously disintegrate into spherical drops as the spherical shape has the minimum surface area. While comparing to the equivalent circular liquid jet, the surface area of elliptical liquid jet with axis-switching segments is larger and such jets tends to disintegrate faster. This is manifested in the breakup curves as the zone of enhanced instability bounded by the lines A–A and C–C in Figs. 14 and 15. Within this zone of enhanced instability, an increase in orifice aspect ratio causes further destabilization of the elliptical liquid jets with relatively lower viscosity. Since an increase in orifice aspect ratio results in an increase in amplitude of axis-switching as illustrated in Fig. 11(a) and (b), surface energy of the jet increases and destabilizes the jet further. However, the presence of viscosity damps axis-switching process quickly for viscous liquids like water–glycerol mixture and all elliptical jets reduce to a more or less circular one after a short distance from the orifice exit. As a result, the effective increase in the jet surface area due to axis-switching process for viscous liquids is significantly less than that of liquids with relatively low viscosity. This renders axis-switching process in elliptical water–glycerol mixture jets too weak to cause a sharp change of the slope of the breakup curve at critical points. In fact breakup curves for elliptical water–glycerol mixture jets show a positive slope even after the critical point (refer Fig. 17) and elliptical jets break axisymmetrically at these flow conditions like circular jets operating in the Rayleigh regime as seen in Fig. 7. Nevertheless, axis-switching indeed enhances their instability and causes their breakup lengths to be reduced less than that of the equivalent circular jet under the same flow conditions. Though $\left(\sqrt{We}\right)_{crit}$ is affected by the aspect ratio, the presence of viscous damping results in the lack of destabilizing effect of aspect ratio in the case of elliptical water–glycerol mixture jets. The stabilizing effect of viscous damping is illustrated through Fig. 19 which is a superimposed plot of the variation of $\left(\sqrt{We}\right)_{crit}$ of water and water–glycerol mixture jets with orifice aspect ratio. Fig. 19 clearly reveals that the effect of viscosity is to delay the critical points in the breakup curves.

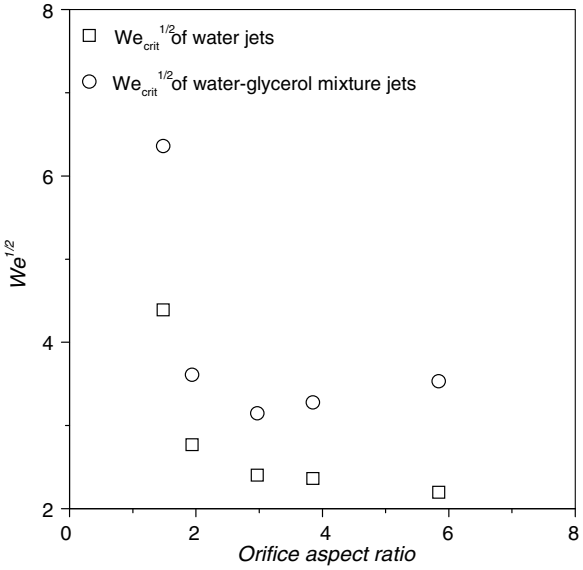

Fig. 19. Variation of $\left(\sqrt{We}\right)_{crit}$ with orifice aspect ratio for water and water–glycerol mixture jets.

5. Conclusions

An experimental study on liquid jets discharging from elliptical orifices of various aspect ratios has been reported. Experiments were carried out with water and water–glycerol mixture of 1:1 by volume as working fluids. Identical experiments were conducted with the circular orifice of same area of cross section as that of the elliptical orifices. Jet velocity at the orifice exit was estimated from the measurement of liquid volume flow rate and the orifice exit area. The simulated flow conditions were extended to Weber number (*We*) as high as 10^4. Photographic techniques were employed to extract details on the flow behavior and breakup process of liquid jets. A systematic analysis was carried out by com-

paring the experimental results obtained for the elliptical orifices with that of the circular orifice.

At very low *We*, liquid jets discharging from the elliptical orifices behave like a circular jet by limiting the influence of elliptical orifice geometry to the immediate vicinity of the orifice exit plane. As *We* increases, the elliptical cross section of liquid jet switches its major and minor axes and the elliptical liquid jet develops axis-switching segments as it flows downstream. The onset of axis-switching process in an elliptical liquid jet is found to be a gradual process occurring within a transition regime covering a range of *We* values. The axis-switching process is visibly seen on elliptical liquid jets at flow conditions beyond the transition regime. However, at very high *We*, jet turbulence and ambient gas medium develop large scale distortions on the jet surface which undermine the effect of axis-switching process. The axis-switching process of elliptical liquid jets was characterized in the present study by obtaining the measurements of axis-switching wavelength of the jet and maximum amplitude of axis-switching. The wavelength of axis-switching is found to be independent of the viscosity of the liquid as well as the aspect ratio of the orifice and it varies significantly along the axis of the jet. The amplitude of axis-switching is strongly dependent on the aspect ratio of the orifice as well the viscosity of the liquid. The effect of viscosity is to cause the decay of axis-switching along the jet and this decay is found to increasing with the aspect ratio of the orifice. The axial variation of the axis-switching wavelength and the non-exponential decay of amplitude near the orifice exit advocates for rigorous studies to understand the role played by orifice exit conditions on the behavior of elliptical liquid jets.

Comparison of breakup curves for elliptical liquid jets with that of the equivalent circular liquid jet reveals that the breakup length of elliptical liquid jets is significantly less than that of the circular jet within a range of *We* at which the former exhibits visible axis-switching process. This unveils the destabilizing role of axis-switching process on elliptical liquid jets. At high *We*, the elliptical orifice geometry lacks its influence on the macroscopic breakup process of liquid jets. The destabilizing effect of axis-switching is found to be weaker in the case of relatively more viscous liquid jets like water–glycerol mixture jet. Additional studies are needed to quantify the details of surface atomization and droplet formation processes.

References

Bechtel, S.E., 1989. The oscillation of slender elliptical inviscid and Newtonian jets: effects of surface tension, inertia, viscosity and gravity. Trans. ASME: J. Appl. Mech. 56, 968–974.

Bechtel, S.E., Forest, M.G., Holm, D.D., Lin, K.J., 1988a. One-dimensional closure models for three-dimensional incompressible viscoelastic free jets: von Karman flow geometry and elliptical cross section. J. Fluid Mech. 196, 241–262.

Bechtel, S.E., Lin, K.J., Forest, M.G., 1988b. On the behavior of viscoelastic free jets with elliptical cross section. J. Non-Newton. Fluid Mech. 27, 87–126.

Bechtel, S.E., Cooper, J.A., Forest, M.G., Petersson, N.A., Reichard, D.L., Saleh, A., Venkataramanan, V., 1995. A new model to determine dynamic surface tension and elongational viscosity using oscillating jet measurements. J. Fluid Mech. 293, 379–403.

Bidone, G., 1829. Experiences sur la forme et sur la direction des veines et des courants d'eau lances par diverses ouvertures. Impremerie Royale, Turin, pp. 1–136.

Blaisot, J.B., Adeline, S., 2000. Determination of the growth rate of instability of low velocity free falling jets. Exp. Fluids 29, 247–256.

Bogy, D.B., 1979. Drop formation in a circular liquid jet. Annu. Rev. Fluid Mech. 11, 207–228.

Bohr, N., 1909. Determination of dynamic surface tension by the method of jet vibration. Philos. Trans. Roy. Soc. Lond. 209, 281–317.

Boussinesq, J., 1877. Mem. Acad. Sci. Paris 23.

Chandrasekhar, S., 1961. Hydrodynamic and Hydromagnetic Stability. Clarendon press, Oxford.

Geer, J.F., Strikwerda, J.C., 1980. Vertical slender jets. J. Fluid Mech. 101, 53–63.

Geer, J.F., Strikwerda, J.C., 1983. Vertical slender jets with surface tension. J. Fluid Mech. 135, 155–169.

Grant, R.P., Middleman, S., 1966. Newtonian jet stability. AIChE J. 12, 669–678.

Green, A.E., 1977. On the steady motion of jets with elliptical sections. Acta Mech. 26, 171–177.

Haenlien, A., 1932. Disintegration of a liquid jet. NACA TM 659.

Hoyt, J.W., Taylor, J.J., 1978. Elliptical water jets. AIAA J. 16, 85–87.

Kasyap, T.V., Sivakumar, D., Raghunandan, B.N., 2008. Breakup of liquid jets emanating from elliptical orifices at low flow conditions. Atomization Spray 18, 645–668.

Lefebvre, A.H., 1989. Atomization and Sprays. Taylor & Francis, London.

Lin, S.P., Reitz, R.D., 1998. Drop and spray formation from a liquid jet. Annu. Rev. Fluid Mech. 30, 85–105.

Magnus, G., 1855. Hydraulische untersuchungen. Ann. Phys. Chem. 95, 1–59.

McHale, R.M., Nurick, W.H., Clapp, S.D., 1971. Injector design criteria using noncircular orifice geometry. J. Spacecraft Rockets 8, 408–410.

Pan, Y., Suga, K., 2006. A numerical study of the breakup process of laminar liquid jets into a gas. Phys. Fluids 18, 1–11.

Phinney, R.E., 1972. Stability of a laminar viscous jet – the influence of initial disturbance level. AIChE J. 18, 432–434.

Phinney, R.E., 1973. Stability of a laminar viscous jet – the influence of an ambient gas. Phys. Fluids 16, 193–196.

Plateau, J., 1873. Statisque experimentale et theorique des liquids soumis aux seules forces moleculaires. Gauthier-Villars, Paris.

Rayleigh, L., 1879. On the capillary phenomena of jets. Proc. R. Soc. Lond. 29, 71–97.

Rayleigh, L., 1890. On the tension of recently formed surfaces. Proc. R. Soc. Lond. 41, 281–287.

Rayleigh, L., 1945. The Theory of Sound, vol. 2. Dover, New York.

Reitz, R.D., 1978. Atomization and other breakup regimes of a liquid jet, Ph.D. Thesis, Princeton University, NJ.

Savart, F., 1833. Memoire sur la constitution des veines liquides lancees par des orifices circulaires en mince paroi. Ann. Chim. 53, 337–386.

Snyder, H.E., Senser, D.W., Lefebvre, A.H., Countinho, R.S., 1989. Drop size measurements in electrostatic paint sprays. IEEE Trans. Ind. Appl. 25, 720–727.

Sterling, M., Sleicher, C.A., 1975. The instability of capillary jets. J. Fluid Mech. 68, 477–495.

Taylor, G.I., 1960. Formation of thin flat sheets of water. Proc. Roy. Soc. Lond. 259A, 1–17.

Weber, C., 1931. Zum zerfall eines flüssigkeitsstrahles. Z. Angrew. Math. Mech. 11, 136–154.

Yang, C., Leong, K.C., 2002. Influences of substrate wettability and liquid viscosity on isothermal spreading of liquid droplets on solid surfaces. Exp. Fluids 33, 728–732.